MTH281 Final Project

Team Number One!
Nicholas Baronowsky, Sebastian Jakymiw, Patrick Phillips

December 13, 2019

Contents

Introduction

In general, the physical behavior of water is extremely complex. Energy can be added and removed by the sun, winds, gravity, the motion of the Earth, or the viscosity of the water itself. These effects combine to produce behavior which is difficult to describe, making necessary the use of various approximations for limiting cases.

The shallow water equations are one such useful approximation for water dynamics where horizontal scales are much greater than vertical. In these cases, surface disturbances and the impact of ground topography beneath the water can be examined in detail. The equations governing these interactions are nonlinear and therefore generally unsolvable by analytic means. However, numerical methods can provide remarkably accurate insight into the behavior of water in these situations. The equations explicitly take into account the water depth, the sea-floor topography, and produce the velocity of the fluid
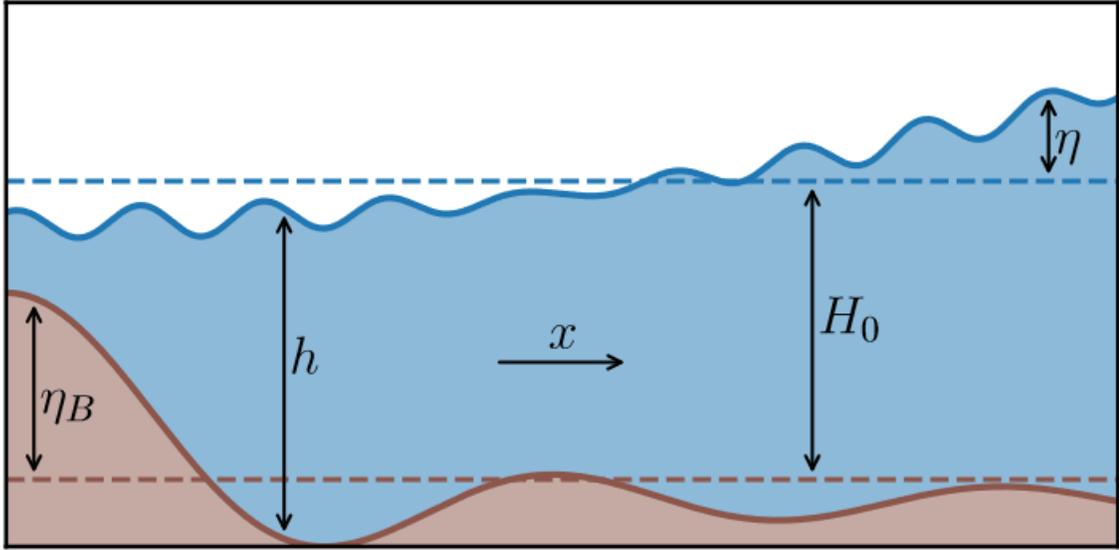
Figure 1: The setup of the 1D wave equation

at a certain point and time. The equations can be used in either one or two dimensions, and are generally valid under the shallow water assumptions and when the depth of the water is nonzero.

1 Analytic Work

1.1 1D

The 1D shallow water equations (without bottom topography) are:

$$
\frac{\partial u}{\partial t} = -u\frac{\partial u}{\partial x} - g\frac{\partial h}{\partial x} \tag{1}
$$
$$
\frac{\partial h}{\partial t} = -\frac{\partial}{\partial x}(uh)
$$

Here u is the positive x velocity, h is the depth of the fluid, and g is the constant acceleration due to gravity. A plot of the 1D shallow water setup can be seen in Figure 1.

a) Linearizing using $u = 0 + \varepsilon\tilde{u}$ and $h = H_0 + \varepsilon\tilde{h}$ leads to

$$\varepsilon\frac{\partial\tilde{u}}{\partial t} = -\varepsilon^2\tilde{u}\frac{\partial\tilde{u}}{\partial x} - g\varepsilon\frac{\partial\tilde{h}}{\partial x}$$

$$\varepsilon\frac{\partial\tilde{h}}{\partial t} = -\varepsilon H_0\frac{\partial\tilde{u}}{\partial x} - \varepsilon^2\frac{\partial}{\partial x}(uh)$$

ε^2 terms are small and can be dropped, leading to the linearized equations

$$\frac{\partial\tilde{u}}{\partial t} = -g\frac{\partial\tilde{h}}{\partial x} \tag{2}$$

$$\frac{\partial\tilde{h}}{\partial t} = -H_0\frac{\partial\tilde{u}}{\partial x} \tag{3}$$

b) Taking a t derivative of 2 and an x derivative of 3, and equating the mixed partial derivatives of $\tilde{h}$, the two equations can be combined into a wave equation:

$$\frac{\partial^2\tilde{u}}{\partial t^2} = H_0 g\frac{\partial^2\tilde{u}}{\partial x^2}$$

Using the ansatz $\tilde{u} = e^{i(Kx-\omega t)}$ yields the dispersion relation $\omega = K\sqrt{H_0 g}$.

c) The characteristic velocity can be obtained from the dispersion relation by dividing the frequency ω by the wavenumber K, or as the square root of the coefficient of $\frac{\partial^2\tilde{u}}{\partial x^2}$ in the PDE. In both cases, the velocity is found to be $\sqrt{H_0 g}$.

d) This relation implies that the velocity of waves in shallow water is proportional to the height of those waves.

e) An appropriate CFL condition given the characteristic velocity $\sqrt{H_0 g}$ would be:

$$\Delta t \leq c\frac{\Delta x}{|\sqrt{H_0 g}|} \tag{4}$$

3

1.2 2D

The 2D shallow water equations are:

$$\frac{\partial u}{\partial t} = -u\frac{\partial u}{\partial x} - v\frac{\partial u}{\partial y} - g\frac{\partial h}{\partial x}$$

$$\frac{\partial v}{\partial t} = -u\frac{\partial v}{\partial x} - v\frac{\partial v}{\partial y} - g\frac{\partial h}{\partial y}$$

$$\frac{\partial h}{\partial t} = -\frac{\partial}{\partial x}(uh) - \frac{\partial}{\partial y}(vh)$$

Here u is again the positive x velocity, h is the depth of the fluid, g is the constant acceleration due to gravity, and now v is the positive y velocity,. Linearizing using the same reference states as in the 1D case, the linear equations obtained are:

$$\frac{\partial \tilde{u}}{\partial t} = -g\frac{\partial \tilde{h}}{\partial x} \tag{5}$$

$$\frac{\partial \tilde{v}}{\partial t} = -g\frac{\partial \tilde{h}}{\partial y} \tag{6}$$

$$\frac{\partial \tilde{h}}{\partial t} = -H_0\left(\frac{\partial \tilde{u}}{\partial x} + \frac{\partial \tilde{v}}{\partial y}\right) \tag{7}$$

Using a similar ansatz $\tilde{u} = \tilde{v} = \tilde{h} = e^{i(Kx+Ly-\omega t)}$ the system reduces to the matrix equation

$$\omega \begin{pmatrix} \tilde{u} \\ \tilde{v} \\ \tilde{h} \end{pmatrix} = \begin{pmatrix} 0 & 0 & gK \\ 0 & 0 & gL \\ H_0K & H_0L & 0 \end{pmatrix} \begin{pmatrix} \tilde{u} \\ \tilde{v} \\ \tilde{h} \end{pmatrix} \tag{8}$$

Substituting the relations $\tilde{u} = \frac{gK}{\omega}\tilde{h}$ and $\tilde{v} = \frac{gL}{\omega}\tilde{h}$, obtained from the first two rows of 8, into the last row of 8, the dispersion relation $\omega = \sqrt{H_0g(K^2+L^2)}$ is found.

4

2 Numerical Work

2.1 Increasing Temporal and Spatial Discretization

In this section, we will analytically derive a second order temporal scheme and fourth order spatial scheme. We will then verify that the higher order scheme in each case has lower error for the same Δt with numerical implementations. In general with these schemes we are trying to find $u(x, t_{n+1})$ given information about $u(x, t_n)$, $u(x, t_{n-1})$, ... Higher order temporal schemes use more of these terms, and the more terms used typically gives a more accurate approximation, but at some computational cost. In general our problem will be of the form

$$\frac{\partial}{\partial t} u = f(u(x, t)). \tag{9}$$

where $f(u(x, t))$ is some function that can be nonlinear and include spatial derivatives. We will denote $f(u(x, t_n))$ as f_n. In this case for f_n we have the 1D shallow water equations that were presented in Section 1 in equation 1.

2.1.1 Second Order Temporal Discretization

With our temporal scheme we want to approximate

$$\int_{t_n}^{t_{n+1}} f_n dt \tag{10}$$

In order to approximate 10, suppose that we know f_n *and* f_{n-1}, as we are trying to construct a second order scheme. From these two points we can find a linear approximation for $f(u)$ centered at $t = t_n$ as

$$f(u(x, t)) \approx f_n + (t - t_n) \frac{f_n - f_{n-1}}{t_n - t_{n-1}} \tag{11}$$

Putting this into the integral in 10, we get

$$\int_{t_n}^{t_{n+1}} f(u) dt = f_n \cdot (t_{n+1} - t_n) + \frac{(t_{n+1} - t_n)^2}{2} \frac{f_n - f_{n-1}}{t_n - t_{n-1}} \tag{12}$$

Assuming that the time steps are of equal magnitude, that is $t_{n+1} - t_n = t_n - t_{n-1} = \Delta t$, we can rewrite 12 as

$$\int_{t_n}^{t_{n+1}} f(u) dt = f_n \cdot \Delta t \left[1 + \frac{1}{2} \frac{\Delta t}{\Delta t} \right] - f_{n-1} \cdot \frac{1}{2} \frac{\Delta t^2}{\Delta t} \tag{13}$$

which simplifies to the second order temporal scheme

$$\int_{t_n}^{t_{n+1}} f(u)dt = \Delta t \left[\frac{3}{2}f_n - \frac{1}{2}f_{n-1}\right] \tag{14}$$

We implemented and then verified that this second order scheme had lower error using the two simple ODEs:

$$\frac{\partial u}{\partial t} = e^{\pi t} \tag{15}$$

$$\frac{\partial u}{\partial t} = \cos \pi t \tag{16}$$

The plots of the analytic solution and temporal scheme approximations of u for each PDE, the absolute error of the estimation from the analytic solution, and the percent error can be seen in Figures 2 and 3.
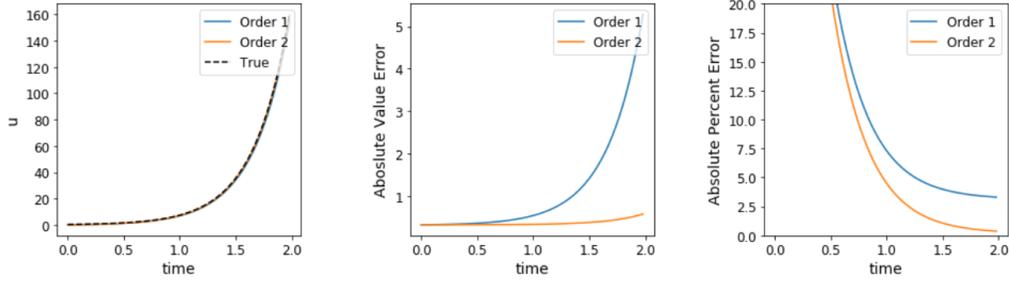

Figure 2: Plot of u=$e^{\pi t}$, along with the solutions to PDE in 15 using the first and second order temporal schemes. Note that the second order scheme is more accurate.
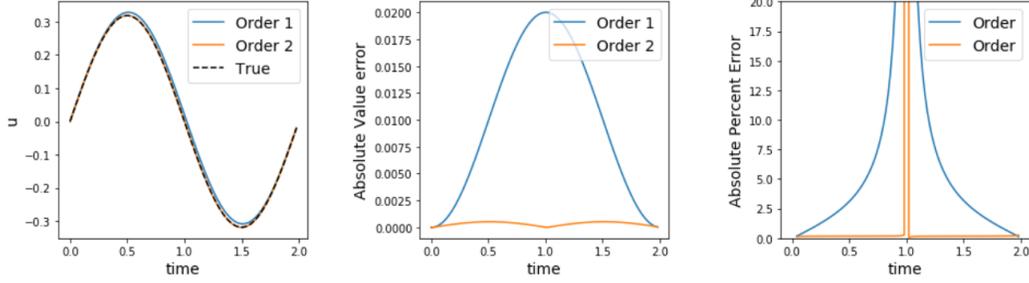
Figure 3: Plot of the analytic solution and approximate solutions to PDE in 16 using the first and second order temporal schemes. Note that the second order scheme is more accurate.

2.1.2 Fourth Order Spatial Discretization

We will derive a fourth order spatial scheme to approximate the derivative $\frac{\partial}{\partial x} u$ for *interior* points x_i. To start, we write Taylor expansions for u at the neighbouring points $x_{i-2}, x_{i-1}, x_{i+1}$, and x_{i+2} centred about x_i as

$$u_{i-2} \approx u_i - 2\Delta x \left.\frac{\partial}{\partial x} u\right|_{x=x_i} + \frac{1}{2} 4\Delta x^2 \left.\frac{\partial^2}{\partial x^2} u\right|_{x=x_i} - \frac{1}{6} 8\Delta x^3 \left.\frac{\partial^3 u}{\partial x^3}\right|_{x=x_i} + \frac{1}{24}\Delta x^4 \left.\frac{\partial^4 u}{\partial x^4}\right|_{x=x_i} + \mathcal{O}(\Delta x^5)$$

$$u_{i-1} \approx u_i - \Delta x \left.\frac{\partial}{\partial x} u\right|_{x=x_i} + \frac{1}{2}\Delta x^2 \left.\frac{\partial^2}{\partial x^2} u\right|_{x=x_i} - \frac{1}{6}\Delta x^3 \left.\frac{\partial^3 u}{\partial x^3}\right|_{x=x_i} + \frac{1}{24}\Delta x^4 \left.\frac{\partial^4 u}{\partial x^4}\right|_{x=x_i} + \mathcal{O}(\Delta x^5)$$

$$\mathrm{u}_i = u_i$$

$$u_{i+1} \approx u_i + \Delta x \left.\frac{\partial}{\partial x} u\right|_{x=x_i} + \frac{1}{2}\Delta x^2 \left.\frac{\partial^2}{\partial x^2} u\right|_{x=x_i} + \frac{1}{6}\Delta x^3 \left.\frac{\partial^3 u}{\partial x^3}\right|_{x=x_i} + \frac{1}{24}\Delta x^4 \left.\frac{\partial^4 u}{\partial x^4}\right|_{x=x_i} + \mathcal{O}(\Delta x^5)$$

7

$$u_{i+2} \approx u_i + 2\Delta x \left.\frac{\partial}{\partial x}u\right|_{x=x_i} + \frac{1}{2}4\Delta x^2 \left.\frac{\partial^2}{\partial x^2}u\right|_{x=x_i} + \frac{1}{6}8\Delta x^3 \left.\frac{\partial^3 u}{\partial x^3}\right|_{x=x_i} +$$

$$\frac{1}{24}\Delta x^4 \left.\frac{\partial^4 u}{\partial x^4}\right|_{x=x_i} + \mathcal{O}(\Delta x^5)$$
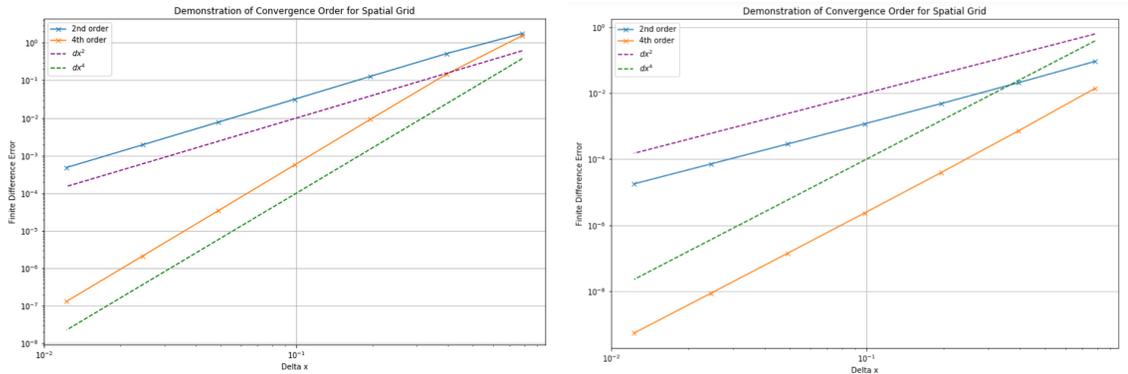
Where we have made the assumption that our grid is uniformly spaced. From the Taylor Expansion above we can find the fourth order scheme by taking a linear combination of $\frac{1}{12}u_{i-2}$, $-\frac{2}{3}u_{i-1}$, $\frac{2}{3}u_{i+1}$, and $-\frac{1}{12}u_{i+2}$. The even terms trivially cancel as they are all positive, and this linear combination is symmetrically positive and negative. The odd terms, except for the first partial derivative term, cancel as well, which results in

$$\Delta x \left.\frac{\partial}{\partial x}u\right|_{x=x_i} + \mathcal{O}(\Delta x^5) = \frac{1}{12}u_{i-2} - \frac{2}{3}u_{i-1} + \frac{2}{3}u_{i+1} - \frac{1}{12}u_{i+2} \qquad (17)$$

Solving for $\Delta x \left.\frac{\partial}{\partial x}u\right|_{x=x_i}$ gives the scheme:

$$\left.\frac{\partial}{\partial x}u\right|_{x=x_i} = \frac{\frac{1}{12}u_{i-2} - \frac{2}{3}u_{i-1} + \frac{2}{3}u_{i+1} - \frac{1}{12}u_{i+2}}{\Delta x} + \underbrace{\mathcal{O}(\Delta x^4)}_{\text{Error term}} \qquad (18)$$

The faster error convergence is verified in the plots shown in Figure 4, where the error between the analytic derivative of two $\cos{()}$ functions is compared to the derivative computed with the fourth order spatial scheme and second order spatial scheme. The additional two lines on these graphs are plots of dx^2 and dx^4. Note that the line representing the fourth order scheme's error is parallel to dx^4 in each graph, implying that the rate of convergence is like dx^4 as predicted. Similarly, the lines for the second order scheme and dx^2 in each graph are parallel.

(a) Graph demonstrating Error Convergence (b) Graph demonstrating Error Convergence
using $f(x) = \cos 3x$ using $f(x) = \cos x$

Figure 4: Plots demonstrating the error convergence of the spatial schemes.
Code used to generate these plots can be found in the folder "Demonstrating
Error Convergence of Higher Order Schemes."

2.2 CFL Condition with Higher Order Model

With our higher order temporal scheme, we have more accurate approxima-
tions, so can use a higher CFL factor. The CFL factor is the value c that
appears in the equation for determining Δt:

$$\Delta t \leq c \frac{\Delta x}{|\sqrt{H_0 g}|} \tag{19}$$

and takes on values $0 < c < 1$. To see how high we can push this CFL factor,
we first run our simulation with a very small CFL, corresponding to a very
small time step. In this case the CFL baseline was taken as 0.001. We then
run simulations of the shallow water equations with CFL factors varying from
0.001 to 0.05 in increments of 0.005 for a total of 10 separate simulations. We
plot the difference in height of the final state from our baseline as a function
of the varying CFL. The plot of this can be see in Figure 5.

It's important to note that this is not a plot of error explicitly, since
there is no analytic solution to compare to here, but comparing against this
baseline simulation that used a very small CFL and Δt is still reasonable.
Based on Figure 5, the difference from the baseline is still reasonably small
when the CFL factor is 0.01, and this is our recommended limit. Lower CFL
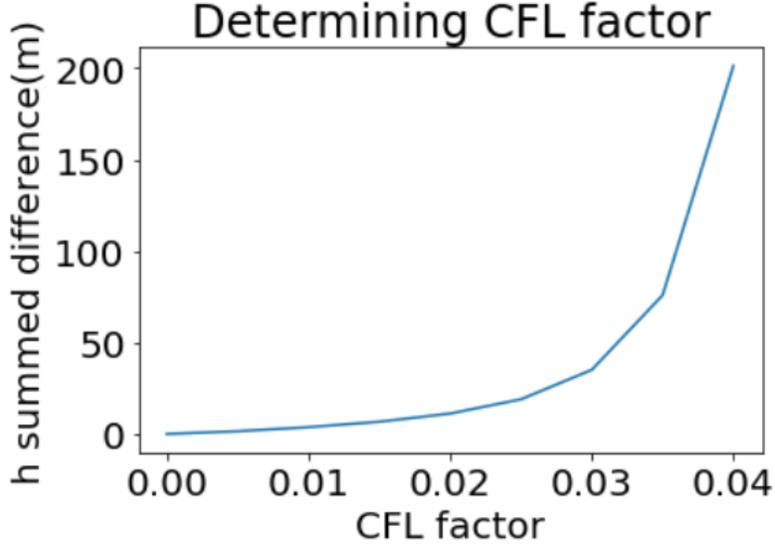factors will have even less error, but it's a tradeoff of efficiency vs. accuracy.

9

Figure 5: Plot of the difference between the baseline simulation and simulations with larger CFL factors. The difference plotted on the y-axis is the sum over all recorded time steps and grid points of the difference between the baseline simulation and the CFL factor plotted on the x-axis.

2.3 Adding Bottom Topography η_b

Bottom topography refers to the deviation of the sea floor from some representative value such as the mean. The physical meaning of η_b can be seen clearly in Figure 1, where negative values of η_b indicate valleys in the sea floor, and positive values indicate hills. The ocean topography η_b can depend on the position (x, y) in the 2D case or just (x) in our 1D case. Importantly, η_b is not a function of time. The 1D shallow water equations with η_b look like

$$\frac{\partial u}{\partial t} = -u\frac{\partial u}{\partial x} - g\frac{\partial}{\partial x}(h + \eta_b)$$
$$\frac{\partial h}{\partial t} = -\frac{\partial}{\partial x}(uh)$$

To incorporate η_b into our model, we have a 1D array called $\eta_b(x)$ which indicates the ocean topography at every point in our spatial grid. Since the partial derivative of η_b with respect to x is nonzero, we evaluate $\frac{\partial}{\partial x}(h + \eta_b)$ using our fourth order spatial scheme.

10

The first test case that we consider to verify that our implementation of adding η_b the ocean topography term is valid is to simply add a very small Gaussian profiled topography of magnitude 10E-5. With this topography, we compare to another simulation with the same set of initial conditions. The results are shown in Figures 6 and 7, and are indistinguishable. Note for replication, the initial conditions used were:

$$h(x,\ 0) = H_0, \quad u(x,\ 0) = 0.03\cos\left(\frac{4\pi x}{L_x}\right) + 0.1\exp\left(-(\frac{x}{0.2})^2\right)$$

Figure 6: Line plot for the initial conditions specified in (b), before topography was added.

Our second validation test is to consider a case with non-trivial topography but a flat water surface, and no initial velocity. The flat surface implies there are no pressure gradients, so no velocity fields should be generated. For this flat surface condition, we want $h + \eta_b =$ constant since this is the height from the mean sea floor. Thus, there would be a uniform pressure gradient, and the system should remain at rest. To do this we take the initial conditions:

$$h(x,0) = \sin\frac{2\pi x}{L_x} + H_0$$

$$\eta_b(x) = -\sin\frac{2\pi x}{L_x}$$

where L_x is the length of the domain, and H_0 is taken to be 10m. Clearly $h(x,0) + \eta_b(x) = H_0$, so this satisfies the flat water condition. The line plots of the position and velocity of the system can be seen in Figure 8, and
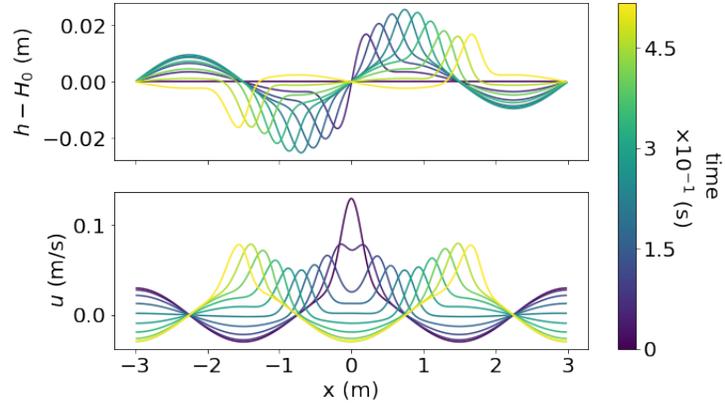
11

Figure 7: Line plot for the initial conditions specified in (b), after small 10E-5 topography was added to simulation. Note that this appears identical to Figure 6.

clearly, nothing is happening as expected, and the water is a constant height of $H_0 = 10(m)$ for all x and t values.
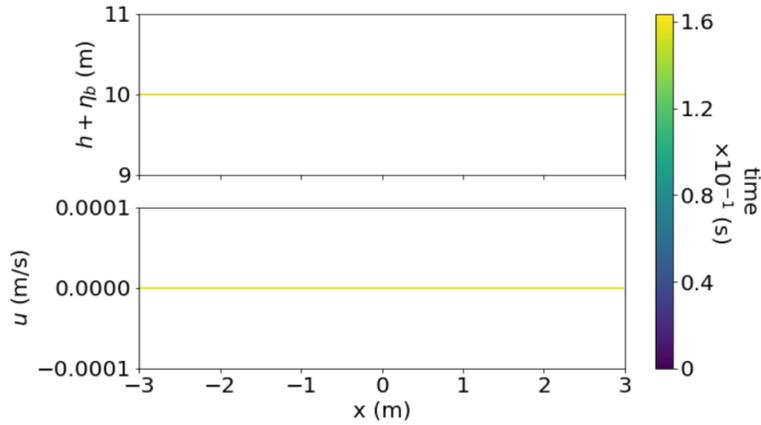

Figure 8: This plot shows the velocity and position of the system as a function of x, with different times color coded. Clearly, the height is flat at a value of $H_0 = 10$, and there is no movement.

12

3 Simulations

3.1 Simulation 1: Zero Initial Velocity

In all these simulations, the following conditions were used:

$$u(x,0) = 0, h(x,0) = H_0 + \eta_0 \exp\{(-(x/L)^2)\}, \eta_B(x) = 0, L = 1/20$$

The two values H_0 and η_0 both modify the height of the initial disturbance in the water. Similar behavior is observed no matter what the parameter values are, just with different magnitudes in both time and height. The only major difference is caused by the sign of η_0.

The system is not symmetric with respect to η_0. Initially, the results look similar to an exact mirror image, but as time progresses the simulation with a negative η_0 appears to show some secondary oscillatory behavior with wave components starting to oscillate closer to the initial disturbance than in the case where η_0 is positive. This is a result of the fact that a negative value corresponds to an initial depression in the water depth, which will cause more oscillatory behavior compared to an initial spike which will average out. The height deviation and velocity plots for an $H_0 = 10$ and $\eta_0 = \pm 0.1 * H_0$ are shown below.
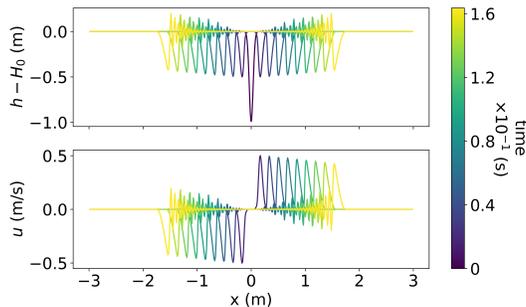

Figure 9: Line Plot for $H_0 = 10, \eta_0 = -0.1 * H_0$

These two parameters both affect the initial disturbance and speed of wave propagation. In particular, as indicated by the derivation of the dispersion relation $\omega = K\sqrt{H_0 g}$, a higher H_0 leads to a much faster characteristic velocity. This difference is seen comparing $H_0 = 100$, where the timescales are on the order of .01, and $H_0 = 10$, where they are an order of magnitude higher.
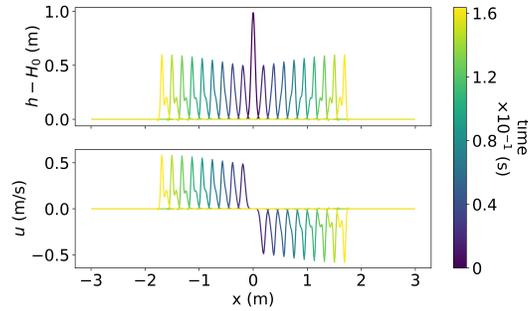
13

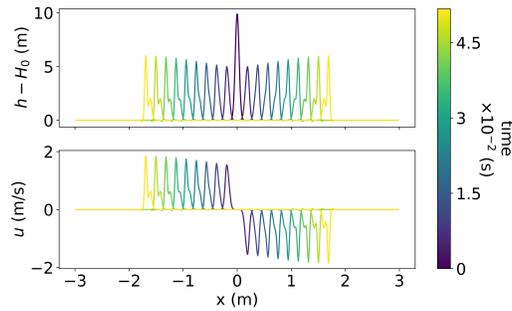Figure 10: Line Plot for $H_0 = 10$, $\eta_0 = 0.1 * H_0$

Figure 11: Line Plot for $H_0 = 100$, $\eta_0 = 0.1 * H_0$

H_0 and η_0 also both cause the height of the first and subsequent waves to vary: lower absolute values of η_0 cause the peak to be diminished, while higher values of H_0 raise it, and vice versa.
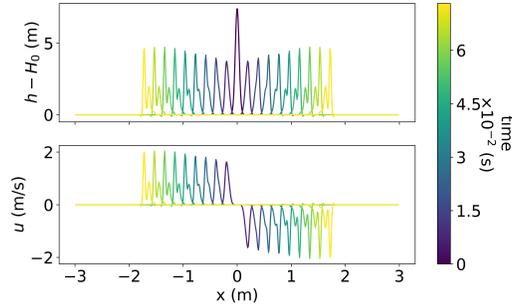
Figure 12: Line Plot for $H_0 = 50$, $\eta_0 = 0.15 * H_0$

3.2 Simulation 2: Constant Initial Velocity

The initial conditions used for the simulations discussed below were $u(x, 0) = U_0, H_0 = 1, h(x, 0) = H_0 + \eta_0 \exp\{-(x/L)^2\}$, and $\eta_0 = 0.02$, where H_0 and η_0 were left fixed and U_0 was varied from simulation to simulation between $[-1, 1]$.
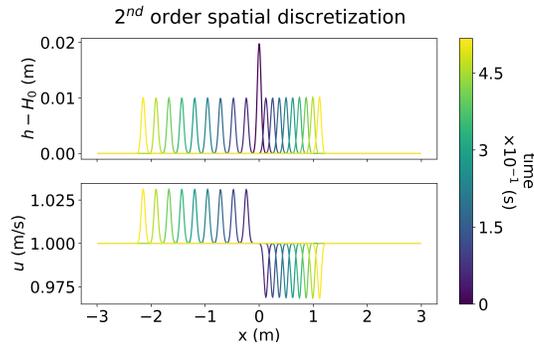

Figure 13: Line Plot for $U_0 = 1$

Physically speaking, the different values for constant initial velocity seem to translate into differences in how far the wave disperses in the line plot. Specifically, for smaller values of U_0, the wave disperses further and more evenly than for larger values. In the relevant plots this difference is most obvious when comparing the change from $U_0 = 1$ (Figure 13) and $U_0 = 0.1$ (Figure 14). For the $U_0 = 1$ case it seems like the larger initial velocity results in waves with shorter wavelengths. This makes sense physically as larger initial velocity results in a larger initial impulse to get the wave motion
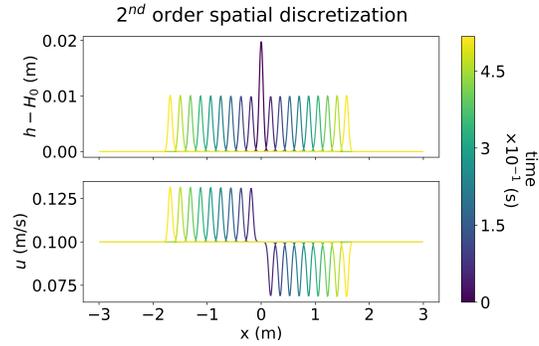
15
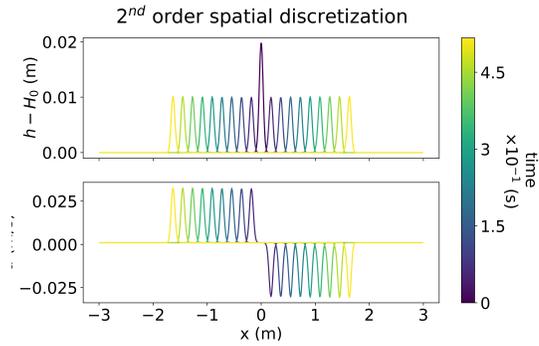
Figure 14: Line Plot for $U_0 = 0.1$

Figure 15: Line Plot for $U_0 = 0.001$

started. That being said, with respect to the global behavior of the system, different values for U_0 do not result in much change.
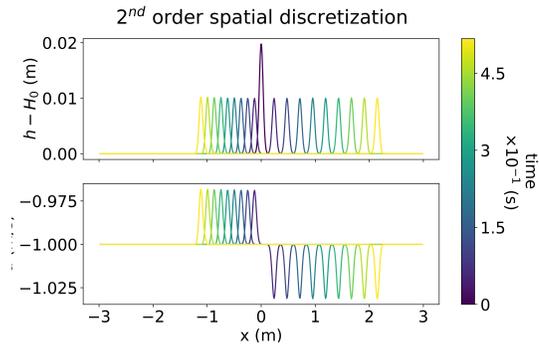

Figure 16: Line Plot for $U_0 = -1$

16

Comparing Figure 16 with Figure 13, setting $U_0 = 1$ or $U_0 = -1$ results in the same general behavior, just in a mirror image over the y axis from each other. Thus this system is symmetric with respect to U_0.

3.3 Simulation 3: Incorporating Bottom Topography

For these simulations, the initial conditions used were: $u(x, 0) = U_0$, $h(x, 0) = H_0$, and $\eta_B(x) = \frac{\Delta\eta}{2} \tanh\left(\frac{|x| - x*}{w}\right)$, with $H_0 = 100$, U_0, between 0 and 1, and $\Delta\eta$ varying. These initial conditions were chosen to test how the same initial wave behaves over varying heights of topography.
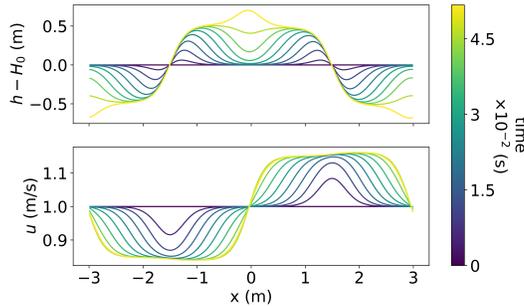

Figure 17: Line Plot for $H_0 = 100$, $U_0 = 1$, $\Delta\eta = 1$

The water appears to mimic the shape of the topography beneath it, starting basically at rest and then rising up as the wave propagates out. Changing values for U_0 and $\Delta\eta$ did not modify the shape of the disturbance, only the magnitude.

This wave behavior matches the implications of the linearization done in the analytic section. The faster-moving waves appear as the initial wave passes over the topography, and reach greater heights than slower moving waves. It would make intuitive sense that a normal water wave, which has a characteristic shape over a flat bottom, would not exhibit any special behavior passing over topography. The appearance would simply mimic the topographical shape.

A wave approaching a sloping coastline from an angle would thus behave in a similar way. Components of the wave reaching the topography first would move slower due to their reduced height, and the whole wave would
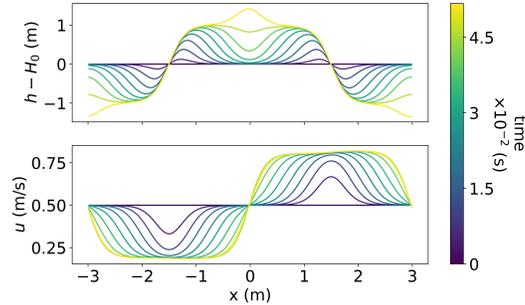
17

Figure 18: Line Plot for $H_0 = 100$, $U_0 = 0.5$, $\Delta\eta = 2$

spread out along the coastline as the components further away reached the angle.

4   Conclusion

During this project we explored the shallow water equations. In the first section we analytically found the dispersion relation in 1D and 2D, and derived the characteristic velocity as well as a CFL condition using linearized versions of the shallow water equations. In the next section we derived and implemented a second order temporal scheme and fourth order spatial scheme to numerically simulate the 1D shallow water equations, and implemented bottom topography. We then tested various CFL factors as well as our implementation of bottom topography. In the final section we used our numerical schemes to simulate the shallow water equations for various initial conditions, exploring the effects of different initial position and velocity configurations as well as the effects of bottom topography. We learned a lot about numerics, PDEs, and shallow water. Thanks to Benjamin Storer for setting up this great project!

4.1   Contributions

Patrick completed the numerical section. He derived (with much help from the notes) and implemented the fourth order spatial scheme and second order temporal scheme. He then used these implementations to demonstrate the reduced error of these schemes. He also worked on determining a reasonable

18

CFL factor and implementing bottom topography.

Nick completed the analytic derivations, as well as the simulations for parts 3.3.1 and 3.3.3.

Sebastian completed the simulations and analysis of results for section 3.3.2 and compiled README data.

All team members verified that the results were valid and accurate, and contributed to organizing and writing the report.